AJNR

Diagnostic accuracy of preoperative quantitative susceptibility mapping for detecting histologic intraplaque hemorrhage in cervical ICA stenosis in patients undergoing carotid endarterectomy

Daisuke Oomori, Yosuke Akamatsu, Ikuko Uwano, Futoshi Mori, Tsuyoshi Matsuda, Ryo Sugimoto, Michiko Suzuki, Shunrou Fujiwara, Masakazu Kobayashi, Makoto Sasaki, Kunihiro Yoshioka, Naoki Yanagawa and Kuniaki Ogasawara

AJNR Am J Neuroradiol published online 24 May 2024
http://www.ajnr.org/content/early/2024/05/24/ajnr.A8356

Published May 24, 2024 as 10.3174/ajnr.A8356

ORIGINAL RESEARCH

Diagnostic accuracy of preoperative quantitative susceptibility mapping for detecting histologic intraplaque hemorrhage in cervical ICA stenosis in patients undergoing carotid endarterectomy

Daisuke Oomori, Yosuke Akamatsu, Ikuko Uwano, Futoshi Mori, Tsuyoshi Matsuda, Ryo Sugimoto, Michiko Suzuki, Shunrou Fujiwara, Masakazu Kobayashi, Makoto Sasaki, Kunihiro Yoshioka, Naoki Yanagawa and Kuniaki Ogasawara

ABSTRACT

BACKGROUND AND PURPOSE: Quantitative susceptibility mapping (QSM) has been proposed to assess intraplaque hemorrhage (IPH) in the carotid artery. The purpose of this study was to compare the diagnostic accuracy of preoperative QSM with that of the conventional T1-weighed (T1W) three-dimensional (3D)-FSE sequence for detecting IPH in cervical ICA stenosis in patients undergoing carotid endarterectomy (CEA) using histology as the reference standard.

MATERIALS AND METHODS: Carotid T1W 3D-FSE and QSM images were obtained from 16 patients with cervical ICA stenosis before CEA. Relative signal intensity (RSI) and susceptibility of the ICA were measured on three axial images including the location of most severe stenosis on T1W 3D-FSE and QSM images, respectively. Three transverse sections of carotid plaques excised by CEA, which corresponded with images on MRI, were stained with H&E, antibody against glycophorin A and Prussian blue, and the relative area (RA) of histologic IPH was calculated.

RESULTS: The correlation coefficient was significantly greater between susceptibility and RA-histologic IPH (ρ = 0.691) than between RSI and RA-histologic IPH (ρ = 0.413; P = .0259). The areas under the receiver operating characteristic curves for detecting histologic sections consisting primarily of IPH (RA-histologic IPH > 40.7%) tended to be greater for susceptibility (0.964) than for T1WI FSE-RSI (0.811). Marginal homogeneity was observed between susceptibility and histologic sections consisting primarily of IPH (P = .0412) but not between T1W FSE-RSI and histologic sections consisting primarily of IPH (P = .1824).

CONCLUSIONS: Pre-CEA QSM detects histologic IPH in cervical ICA stenosis more accurately than preoperative T1W 3D-FSE imaging.

ABBREVIATIONS: QSM = quantitative susceptibility mapping; IPH = intraplaque hemorrhage; T1W = T1-weighed; 3D = three-dimensional; CEA = carotid endarterectomy; RSI = relative signal intensity; RA = relative area.

Received month day, year; accepted after revision month day, year.
From the Department of Neurosurgery (D.O., Y.A., S.F., M.K., K.O.), Department of Molecular Diagnostic Pathology (R.S., N.Y.), Department of Radiology (M.S., K.Y.), and Division of Ultrahigh Field MRI, Institute for Biomedical Sciences (I.U., F.M., T.M., M.S.), Iwate Medical University School of Medicine, Yahaba-cho, Japan.

This work was supported in part by Grants-in-Aids from the Scientific Research KAKEN from the Japan Society for the Promotion of Science (Nos. 21K09108, 21K09157, and 17H04304) and Grants-in-Aids from the National Hospital Organization Kamaishi Hospital KENKYUHI.

For correspondence or reprints contact: Kuniaki Ogasawara, M.D., Department of Neurosurgery, Iwate Medical University, Idaidoori 2-1-1, Yahaba-cho, 020-8505, Japan; kuogasa@iwate-med.ac.jp.

SUMMARY SECTION

PREVIOUS LITERATURE: Vulnerable atherosclerotic plaques including intraplaque hemorrhage (IPH) in the carotid artery are related to subsequent or recurrent cerebrovascular ischemic events. Identification of IPH also may allow stratification of the risks of intraprocedural ischemic events in patients undergoing carotid endarterectomy (CEA) or stenting. Quantitative susceptibility mapping (QSM) produced from the T2*-weighted magnitude/phase has been used to assess the presence of hemorrhage, iron, and calcification in the brain. A recent ex vivo study showed that QSM for carotid plaque excised by CEA can quantify the degree of histologic intraplaque hemorrhage and iron deposition.

KEY FINDINGS: The correlation coefficient was significantly greater between susceptibility of carotid plaque on pre-CEA QSM and relative area (RA) of histologic IPH (ρ = 0.691) in excised carotid plaque than between relative signal intensity of carotid plaque on preoperative T1-weighted three-dimensional-FSE imaging and RA-histologic IPH (ρ = 0.413; P = .0259).

KNOWLEDGE ADVANCEMENT: Pre-CEA QSM detects histologic IPH in carotid artery stenosis more accurately than

preoperative T1-weighted three-dimensional-FSE imaging, suggesting that the former may allow more accurate stratification of the risk of further ischemic events for carotid stenosis as well as the risk of embolic events during surgical interventions than the latter imaging.

INTRODUCTION

Vulnerable atherosclerotic plaques in the carotid artery are related to subsequent or recurrent cerebrovascular ischemic events[1] and often contain intraplaque hemorrhage (IPH).[1,2] For patients with symptomatic and severe stenosis of the cervical ICA, carotid endarterectomy (CEA) or carotid artery stenting can effectively prevent further stroke.[3-5] Identification of IPH in carotid plaques is reportedly useful for specifying revascularization candidates who would be better candidates for CEA than for carotid artery stenting, as carotid plaques consisting primarily of IPH are associated with increased rates of adverse events such as intraoperative procedure-related cerebral infarction among patients undergoing carotid artery stenting but not CEA.[6] In terms of CEA, the intraoperative development of emboli is also strongly associated with vulnerable carotid plaques primarily comprising IPH.[7,8] In such situations, early clamping of the common and external carotid arteries before exposure of the ICA with fragile plaque consisting primarily of IPH prevents the development of new postoperative ischemic events due to embolism.[9] In terms of carotid artery stenting for vulnerable carotid plaques consisting primarily of IPH, balloon occlusion of the common and external carotid arteries as compared with filter protection for the ICA distal to the stenotic lesion reduces the risk of cerebral embolism.[10,11] Identification of IPH may thus allow stratification of the risks of intraprocedural ischemic events in patients undergoing CEA or carotid artery stenting.

IPH is generally assessed using MR imaging based on T1-weighted (T1W) sequences such as cardiac-gated black-blood FSE, MPRAGE, three-dimensional (3D) TOF MRA, and 3D-FSE because these sequences exploit the T1-shortening induced by the presence of methemoglobin.[7,12-16] However, old chronic IPH may contain iron-rich hemosiderin, which can cause IPH to appear hypointense on T1W images due to strong intravoxel signal dephasing, potentially leading to misdetection of IPH. In addition, the disadvantage of this MR plaque imaging includes displaying only methemoglobin as high signal intensity[17] and the need for reference tissue such as surrounding muscles.

Quantitative susceptibility mapping (QSM) is a post-processing technique for quantifying magnetic susceptibility from the T2*-weighted magnitude/phase, which is easily obtained by commercial scanners.[18] This technique has been used to assess the presence of hemorrhage, iron, and calcification in the brain.[19-21] A recent ex vivo study showed that QSM for carotid plaque excised by CEA can quantify the degree of histologic intraplaque hemorrhage and iron deposition.[22] On the other hand, comparisons between data from preoperative carotid QSM and histologic findings from excised carotid plaque in patients undergoing CEA have been reported only on a preliminary basis.[23,24]

Given this background, the purpose of the present study was to determine the diagnostic accuracy of preoperative QSM for detecting histologic intraplaque hemorrhage in cervical ICA stenosis by way of comparison with findings from preoperative T1W 3D-FSE imaging in patients undergoing CEA.

MATERIALS AND METHODS

The protocol for the present prospective observational study was reviewed and approved by our institutional ethics committee. Written, informed consent was obtained from all participants or their next of kin before the study began.

Patients

Patients who underwent CEA at our hospital and met the following inclusion criteria were prospectively enrolled: 1) symptomatic (ischemic episodes present ≥ 2 weeks and < 6 months before the patient visited our institution) ipsilateral ICA stenosis ≥ 70% or asymptomatic ipsilateral ICA stenosis ≥ 80%, as defined by the NASCET in association with DSA via arterial catheterization; and 2) a mRS score of 0–2 before surgery. Patients who satisfy the above criteria usually undergo CEA rather than carotid artery stenting at our institute.

MR Plaque Imaging and Data Processing

MRI for cervical ICA stenosis was performed using a 3-T MRI scanner (SIGNA Architect; GE Healthcare, Waukesha, WI) with a 19-channel head neck coil within 7 days before surgery. First, carotid plaque imaging was obtained using a sagittal T1W 3D-FSE sequence with variable flip angle and the following scan parameters: TR, 500 ms; TE, 10 ms; echo train length, 14; FOV, 256 × 256 mm^2; acquisition matrix size, 224 × 224; image matrix size, 512 × 512; slice thickness, 1.4 mm; voxel size after zero-fill interpolation, 0.5 × 0.5 × 0.7 mm^3; scan time, 1 minute 59 seconds. The location of most severe stenosis in the ICA ipsilateral to the scheduled CEA was visually determined on T1W 3D-FSE images.

Subsequently, source data of carotid plaque imaging for QSM were also obtained with a 3D radiofrequency-spoiled gradient-echo sequence using the same 3-T MRI scanner; the parameters except TE and matrix were as follows: TR, 56 ms; flip angle, 15°; FOV, 200 × 200 mm^2; slice thickness, 1.0 mm; and parallel imaging factor, 1.5. Imaging covered from 20 mm proximal to 20 mm distal from the location of most severe stenosis as determined on T1W 3D-FSE images. Eight patients were preliminarily scanned to determine optimal TEs (3.1/6.1/9.0/12.0/15.0/17.9 ms), number of excitations (1)

and acquisition matrix size (200 × 200) (Online Supplemental Data). Final voxel size and scan time were 0.39 × 0.39 × 0.5 mm^3 after zero-fill interpolation and 3 min 59 s, respectively. QSM images were generated from magnitude and phase images of all TEs through the following reconstruction techniques. First, region-growing phase unwrapping and phase averaging with magnitude weighting were performed on phase images. Regularization-enabled sophisticated harmonic artifact reduction for phase data was then performed as a background field removal.[25] For dipole inversion, least-squares estimation with adaptive edge-preserving filtering was used.[26] We implemented in-house codes (Fujifilm Healthcare, Tokyo, Japan) to semi-automatically calculate final QSM images for objectively obtaining all images using SPM12 (Wellcome Centre for Human Neuroimaging, London) and MATLAB (MathWorks, MA). The implemented codes are not publicly available, but the present procedures were undertaken in accordance with descriptions in previous studies.[27,28]

In addition to a reformatted axial image at the location of most severe stenosis in the ICA, reformatted axial images at 5 mm proximal and 5 mm distal from the location of most severe stenosis were also generated on T1W 3D-FSE images. One examiner (D.O.) blinded to patient information manually traced the circumference of the ICA and adjacent sternomastoid muscle on these three reformatted axial images for each patient (Figs. 1, 2).

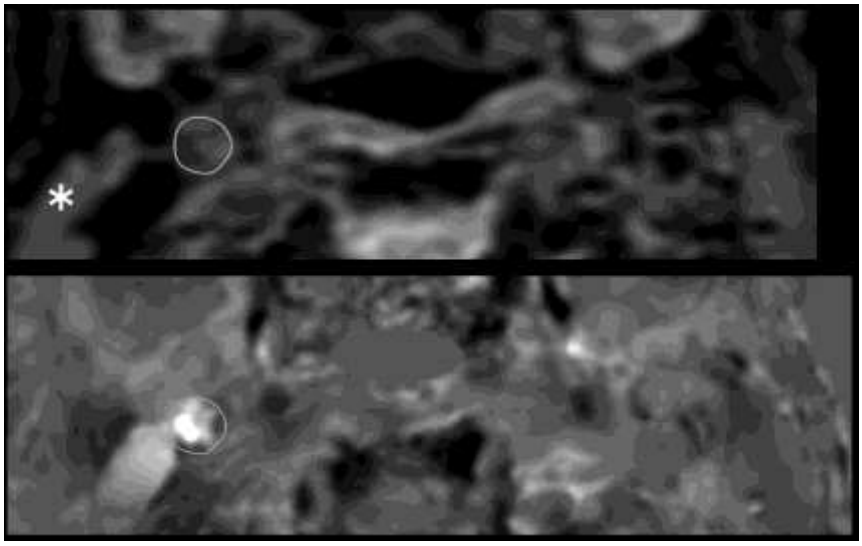

FIG 1. Preoperative reformatted axial MR images with the location of most severe stenosis in the right cervical ICA and histologic transverse sections of carotid plaques excised by carotid endarterectomy from a 61-year-old male patient with minor strokes complicated by left-sided hemiparesis. **A)** Whereas signal intensity of the plaque in the right cervical ICA (grey circle) appears equal to that of the sternocleidomastoid muscle (white asterisk) on T1-weighted (T1W) 3D-FSE image (upper image), its susceptibility (grey circle) is obviously high when compared with that of the background on quantitative susceptibility mapping (lower image).

B) Left, middle, and right images represent histologic sections stained with H&E, antibody against glycophorin A, and Prussian blue, respectively. The circumference of the whole plaque is traced with a black line on a histologic section stained with H&E (left image). Areas positive for antibody against glycophorin A (middle image) and Prussian blue staining (right image) are also traced with red and yellow lines, respectively. Each black asterisk indicates a true lumen of the ICA.

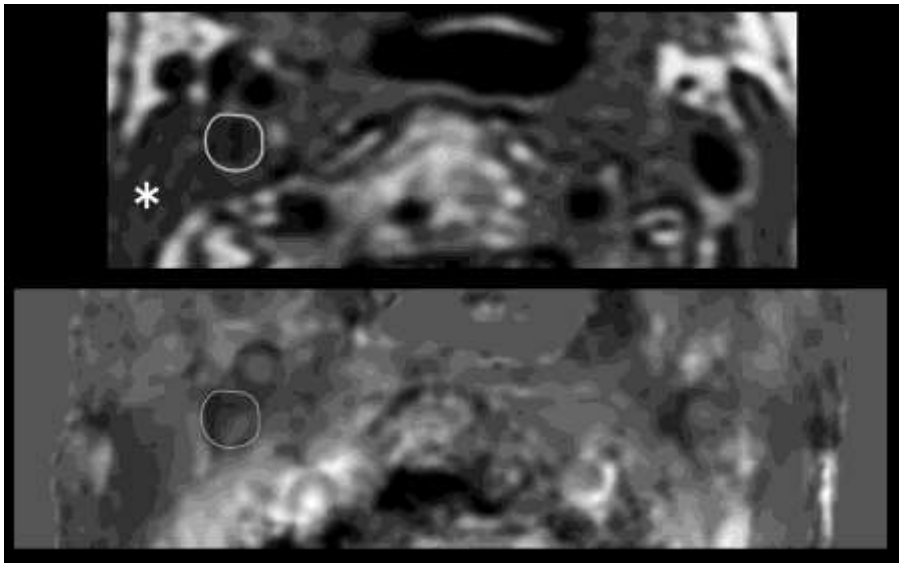

FIG 2. Preoperative reformatted axial MR images with the location of most severe stenosis in the right cervical ICA and histologic transverse sections of carotid plaques excised by carotid endarterectomy for a 77-year-old male patient with minor strokes complicated by left-sided hemiparesis. **A)** Signal intensity of the plaque in the right cervical ICA (white circle) appears equal to that of the sternocleidomastoid muscle (white asterisk) on T1W 3D-FSE image (upper image). Its susceptibility (grey circle) also appears equal to or lower than that of the background on quantitative susceptibility mapping (lower image).

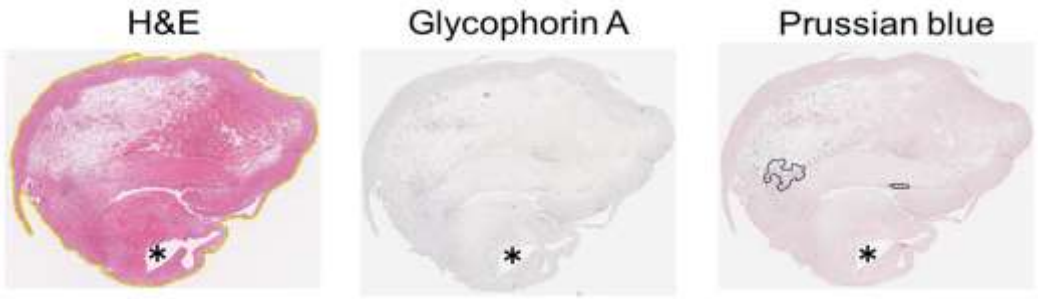

B) Left, middle, and right images represent histologic sections stained with H&E, antibody against glycophorin A and Prussian blue, respectively. No areas positive for antibody against glycophorin A are observed (middle image). The circumference of the whole plaque is traced as a yellow line on a histologic section stained with HE (left image). Areas positive for Prussian blue staining are also traced with black lines (right image). Each black asterisk indicates a true lumen of the ICA.

When tracing the circumference of the ICA, the true lumen was included. Signal intensities of the ICA and adjacent sternomastoid muscle were measured on each reformatted axial image using OsiriX MD (Pixmeo, Geneva, Switzerland). Images were randomized and the ICA and muscle were traced 3 times on each reformatted axial image. The resulting signal intensity values were averaged, then the average signal intensity of the ICA was divided by that of the muscle on each reformatted axial image. This value was defined as the T1W FSE-relative signal intensity (RSI).

Three reformatted axial images from T1W 3D-FSE images were automatically transferred to QSM and three ROIs on the ICA traced on T1W 3D-FSE images were automatically superimposed on QSM for each patient. The susceptibility value was measured in each ROI of the ICA (Figs. 1, 2).

Intraoperative Management and Histologic Analysis for Carotid Plaque

CEA was performed under general anesthesia. Intraoperative transcranial Doppler monitoring (EME Pioneer TC2020 system, Nicolet Vascular, Colorado) was performed for insonation of the middle cerebral artery ipsilateral to the carotid artery undergoing CEA.[12] When microembolic signals were observed on transcranial Doppler during exposure of the carotid arteries, early clamping of the common and external carotid arteries was performed.[9] Based on the results of intraoperative electroencephalography with a 12-channel montage, some patients received placement of an intraluminal shunt.[29]

Carotid plaque was excised en bloc without cutting into the plaque and was fixed in 10% neutral-buffered formalin solution. The location of most severe stenosis determined on T1W 3D-FSE images was visually identified on the exterior of the specimen by comparing the shape on T1W 3D-FSE images with that of the specimen. Locations 5 mm proximal and 5 mm distal from the location of most severe stenosis were also determined on the exterior of the specimen. Next, the specimen was embedded in paraffin and transverse 3-μm-thick sections of the specimen were carefully cut in the above-mentioned three locations. These three transverse sections in each plaque were stained with H&E, antibody against glycophorin A, sialoglycoprotein on the erythrocyte membrane to detect erythrocytes, and Prussian blue to visualize ferric

iron (Fe3+) to identify hemosiderin deposits indicative of chronic hemorrhage. Stained sections of the specimen were transferred to a virtual slide system (Aperio Digital Pathology; Leica Biosystems, Wetzlar, Germany) and all subsequent procedures were performed on this system.

One pathologist (R.S.) blinded to patient information manually traced the circumference of the whole plaque on a histologic section stained with H&E and automatically quantified the area of the whole plaque using image analysis software (Aperio ImageScope; Leica Biosystems, Wetzlar, Germany) (Figs. 1, 2). When tracing the circumference of the whole plaque, the true lumen was included (Figs. 1, 2). The same pathologist also manually traced the circumferences of areas positive for Prussian blue or antibody against glycophorin A, respectively, and quantified these areas in the same fashion (Figs. 1, 2). In addition, in the same histologic section, circumferences of areas positive for both Prussian blue and antibody against glycophorin A were manually traced and the areas were automatically quantified. Finally, in each histologic section, the relative area of histologic IPH (RA-histologic IPH) (%) was calculated as follows: 100 × (areas positive for Prussian blue plus areas positive for antibody against glycophorin A minus areas positive for both) / area of the whole plaque. Any histologic section showing RA-histologic IPH > 40.7% was defined as plaque consisting primarily of IPH.[12]

Statistical Analysis (Online Supplemental Data)

RESULTS

A total of 24 patients were included in the present study: eight patients served to determine optimal parameters for preoperative QSM plaque imaging of cervical ICA and the remaining 16 patients underwent preoperative QSM plaque imaging using optimally determined parameters and histologic analysis of the excised carotid plaque.

These 16 male patients had a mean age of 72 ± 6 years (range, 61–80 years). Twelve patients had ipsilateral carotid territory symptoms, and 4 had asymptomatic ICA stenosis. Mean ICA stenosis was 89 ± 8% (range, 75–95%). Three reformatted axial images including the locations of most severe stenosis and 5 mm proximal and distal from the location of most severe stenosis were obtained from T1W 3D-FSE images and QSM in all 16 patients. Three histologic sections corresponding to reformatted axial images on T1W 3D-FSE were obtained from 15 patients. In the remaining patient, the distance between the location of most severe stenosis and the distal end of the plaque was 3 mm, so only two histologic sections (the location of most severe stenosis and 5 mm proximal to the location of most severe stenosis) were obtained. Forty-seven reformatted axial images and histologic sections were thus analyzed.

A significant positive correlation was observed between RA-histologic IPH and T1WI FSE-RSI (ρ = 0.413; P = .0052) or susceptibility (ρ = 0.691; P < .0001) for the 47 images and sections (Fig. 3).

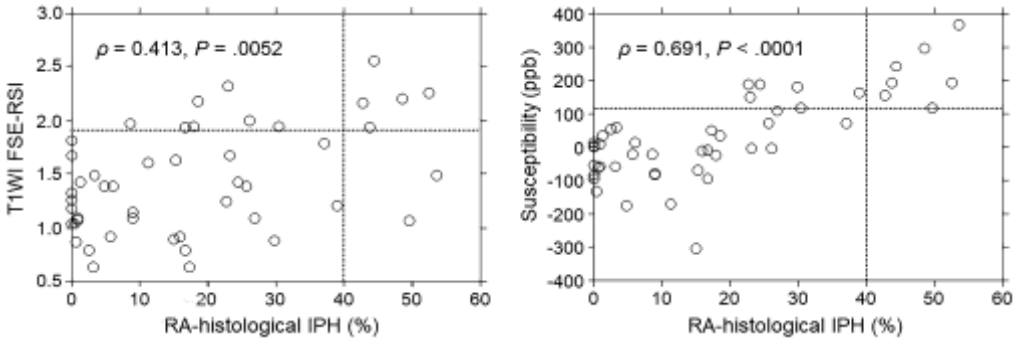

FIG 3. Comparisons of relative area (RA)-histologic intraplaque hemorrhage (IPH) and T1W FSE-relative signal intensity (RSI) (left graph) or susceptibility on quantitative susceptibility mapping (right graph) for each histologic section and each MR image. Each vertical dotted line denotes the cutoff point for indicating a histologic section consisting primarily of IPH (40.7% for RA-histologic IPH) and each horizontal dotted line denotes the cutoff point lying closest to the upper left corner of the receiver operating characteristic curve for detecting a histologic section consisting primarily of IPH (1.90 for T1W FSE-RSI, 115.7 for susceptibility).

The latter coefficient was significantly greater than the former (P = .0259). Because ranges of values differed considerably among the three groups (0–53.6 for RA-histologic IPH; 0.63–2.56 for T1W FSE-RSI; -302.5–365.4 for susceptibility), each value was standardized using the following formula: (a value minus mean of the referenced group)/SD of the referenced group. Bland–Altman analysis was performed using these standardized values (Online Supplemental Data). No constant bias was detected for RA-histologic IPH and T1W FSE-RSI (95%CI of difference, -2.10─2.10) or susceptibility (95%CI of difference, -1.46─1.46). Further, no proportional bias was identified for RA-histologic IPH and T1W FSE-RSI (slope-of-regression equation, 0.04) or susceptibility (slope-of-regression equation, -0.04). Generalized linear mixed-effects models with a subject random intercept revealed a significant relationship between RA-histologic IPH and T1W FSE-RSI (P < .05) or susceptibility (P < .05).

Of the 47 histologic sections analyzed, 7 (15%) were determined to show plaque consisting primarily of IPH. Areas under the ROC curves for histologic sections consisting primarily of IPH tended to be greater for susceptibility (0.964; 95%CI, 0.910–1.000) than for T1W FSE-RSI (0.811; 95%CI, 0.607–1.000), although areas did not differ significantly between the two (difference between areas, 0.154; P = .0820) (Fig. 4).

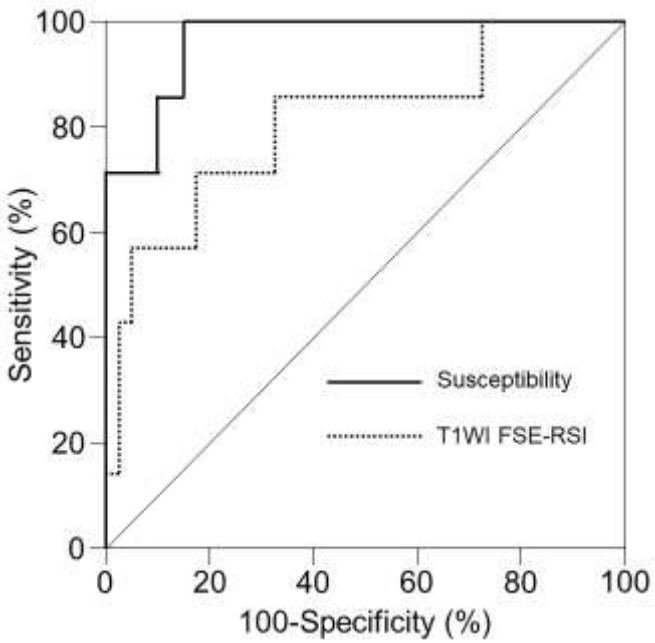

FIG 4. Receiver operating characteristic curves used to compare the accuracy of T1WI FSE-RSI and susceptibility for detecting a histologic section consisting primarily of IPH. Areas under the curves tend to be greater for susceptibility (solid line) than for T1W FSE-RSI (dotted line), although pairwise comparison analysis shows no significant difference between the two.

Sensitivity, specificity, and positive and negative predictive values for the cutoff point lying closest to the upper left corner of the ROC curve for the detection of histologic sections consisting primarily of IPH were 71%, 83%, 42%, and 94%, respectively, for T1W FSE-RSI (cutoff, 1.90) and 100%, 85%, 54%, and 100%, respectively, for susceptibility (cutoff, 115.7 ppb). Marginal homogeneity was observed between histologic sections consisting primarily of IPH and susceptibility (P = .0412), but not between histologic sections consisting primarily of IPH and T1W FSE-RSI (P = .1824).

DISCUSSION

The results of this study demonstrated that pre-CEA QSM can detect histologic intraplaque hemorrhage in cervical ICA stenosis more accurately than preoperative T1W FSE imaging among patients undergoing CEA.

Five distinct stages of hemorrhage can be defined: hyperacute (intracellular oxyhemoglobin); acute (intracellular deoxyhemoglobin); early subacute (intracellular methemoglobin); late subacute (extracellular methemoglobin); and chronic (ferritin and hemosiderin).[17] The short T1 of methemoglobin is due to the paramagnetic dipole-dipole interaction, and MR imaging based on T1-weighted sequences such as T1W FSE displays only methemoglobin before and after red cell lysis as high signal intensity.[17] The magnetic susceptibility effect is responsible for the short T2 observed when deoxyhemoglobin, methemoglobin, or hemosiderin exists intra- or extracellularly.[17] This T2 shortening due to magnetic susceptibility effects is enhanced on higher-field-strength systems and on the gradient-echo images used in the present study.[17] QSM is thus theoretically superior to T1W FSE on 3-T MRI for detecting IPH that may comprise oxyhemoglobin, deoxyhemoglobin, methemoglobin, and/or hemosiderin. Our results were compatible with this hypothesis. On the other hand, antibody against glycophorin A staining is used to detect the erythrocyte membrane rather than iron, suggesting that antibody against glycophorin A staining may reflect oxyhemoglobin, deoxyhemoglobin, and methemoglobin prior to red cell lysis. Prussian blue staining visualizes only hemosiderin deposits. Even a combination of these two stains may not reflect extracellular methemoglobin. Differences among staining by these methods represented the most serious limitations in the present study. Whereas Wang et al. also showed a significant correlation between QSM-detected and histologic IPH areas in patients with carotid stenosis, IPH areas detected by QSM and T1W FSE showed good agreement between the two methods (Online Supplemental Data).[24] Differences between the latter results and our data may be attributable to methodological differences, such as determination of the presence and area of IPH on QSM or T1W FSE.

A previous study compared the development of transcranial Doppler-based microembolic signals during exposure of the carotid arteries in carotid endarterectomy with the percentage area of IPH in the carotid plaque and showed that the cutoff point lying closest to the left upper corner of the ROC curve for the percentage area of IPH in predicting the development of microembolic signals was 40.7%.[12] Based on that finding, we defined histologic sections showing RA-histologic IPH > 40.7% as consisting primarily of IPH. Based on this, the sensitivity and specificity for predicting carotid plaque consisting primarily of IPH were significantly greater for QSM than for T1W FSE, and both the sensitivity and negative predictive value of QSM for such predictions were 100%. These data suggested that carotid plaque imaging using QSM may allow more accurate stratification of the risk of further ischemic events for patients with cervical carotid stenosis, as well as the risk of embolic events during surgical interventions for cervical carotid stenosis, than imaging using T1W FSE. Based on these data, we propose the following practical clinical algorithm for determining whether carotid artery stenting or CEA is indicated: when susceptibility on the stenotic lesion of the affected carotid artery exceeds the

cutoff (115.7 ppb), the stenotic lesion is determined to consist primarily of IPH and, in principle, CEA is recommended over carotid artery stenting. In CEA for such lesions, early clamping of the common and external carotid arteries before exposure of the ICA is recommended. When carotid artery stenting is applied for such lesions, balloon occlusion of the common and external carotid arteries rather than filter protection for the ICA distal to the stenotic lesion is recommended.

QSM clearly displays hemorrhage, iron, and calcification, but does not depict other tissues.[19-21] For this reason, carotid plaque cannot always be identified on QSM alone. In the present study, the location of carotid plaque was visually identified on T1W 3D-FSE images and QSM of the identified carotid plaques was performed. An additional scan time of 2 min (total scan time, 6 min) is thus needed for the detection of IPH in cervical ICA stenosis using QSM.

In addition to the limitations already listed above, some other issues need to be kept in mind when interpreting our results. First, the number of patients included in this study was quite small. Second, carotid plaque usually comprises lipid-rich necrotic core, fibrous tissue and calcifications other than IPH. Regions of interest in the ICA might include calcifications that are displayed as hypointensity on QSM due to their diamagnetic properties. This characteristic of calcifications may reduce the accuracy of detecting IPH using QSM. However, calcifications on histologic sections reportedly tend to be smaller than the voxel size of $0.2 \times 0.2 \times 1.0$ mm^3 on QSM images.[22] The voxel size on QSM images in the present study ($0.39 \times 0.39 \times 0.5$ mm^3) was similar, and paramagnetic hemoglobin or hemosiderin or both may exert stronger effects than diamagnetic calcifications. Third, the location of most severe stenosis determined on T1W 3D-FSE images was visually identified from the exterior of the specimen excised in CEA by comparing the shape of the specimen with that on T1W 3D-FSE images. Therefore, histologic sections may not have exactly matched the corresponding MR image. Lastly, the circumferences of the ICA and whole plaque were traced manually rather than automatically on reformatted axial MR images and on histologic sections, respectively. Further, both circumferences included the true lumen, which might have minimally affected our data because only patients with severe stenosis of the ICA participated in this study. Whether our findings are applicable for moderate or mild ICA stenosis should be examined in future work.

CONCLUSIONS

Pre-CEA QSM detects histologic intraplaque hemorrhage in cervical ICA stenosis more accurately than preoperative T1W FSE imaging in patients undergoing CEA. The practical clinical algorithm for determining whether carotid artery stenting or CEA is indicated based on this finding may reduce the incidence of development of intraoperative embolism or intraoperative procedure-related cerebral infarction.

REFERENCES

1. Liu XS, Zhao HL, Cao Y, et al. Comparison of carotid atherosclerotic plaque characteristics by high-resolution black-blood MR imaging between patients with first-time and recurrent acute is chemic stroke. *AJNR Am J Neuroradiol* 2012;33:1257–61

2. Saam T, Hetterich H, Hoffmann V, et al. Meta-analysis and systematic review of the predictive value of carotid plaque hemorrhage on cerebrovascular events by magnetic resonance imaging. *J Am Coll Cardiol* 2013;62:1081–91

3. Rothwell PM, Eliasziw M, Gutnikov SA, et al. Carotid Endarterectomy Trialists' Collaboration. Analysis of pooled data from the randomised controlled trials of endarterectomy for symptomatic carotid stenosis. *Lancet* 2003;361:107–16

4. Endarterectomy for asymptomatic carotid artery stenosis. Executive Committee for the Asymptomatic Carotid Atherosclerosis Study. *JAMA* 1995;273:1421–28

5. Brott TG, Hobson RW 2nd, Howard G, et al. Stenting versus endarterectomy for treatment of carotid-artery stenosis. *N Engl J Med* 2010; 363:11–23

6. Brinjikji W, Huston J 3rd, Rabinstein AA, et al. Contemporary carotid imaging: from degree of stenosis to plaque vulnerability. *J Neurosurg* 2016; 124: 27–42

7. Altaf N, Beech A, Goode SD, et al. Carotid intraplaque hemorrhage detected by magnetic resonance imaging predicts embolization during carotid endarterectomy. *J Vasc Surg* 2007;46:31–36

8. Sitzer M, Müller W, Siebler M, et al. Plaque ulceration and lumen thrombus are the main sources of cerebral microemboli in high grade internal carotid artery stenosis. *Stroke* 1995;26:1231–33

9. Kobayashi M, Ogasawara K, Inoue T, et al. Urgent endarterectomy using pretreatment with free radical scavenger, edaravone, and early clamping of the parent arteries for cervical carotid artery stenosis with crescendo transient ischemic attacks caused by mobile thrombus and hemodynamic cerebral ischemia. *Neurol MedChir (Tokyo)* 2007;47:121–25

10. Bijuklic K, Wandler A, Hazizi F, et al. The PROFI study (Prevention of Cerebral Embolization by Proximal Balloon Occlusion Compared to Filter Protection During Carotid Artery Stenting): a prospective randomized trial. *J Am Coll Cardiol* 2012;59:1383–89

11. Stabile E, Sannino A, Schiattarella GG, et al. Cerebral embolic lesions detected with diffusion-weighted magnetic resonance imaging following carotid artery stenting: a meta-analysis of 8 studies comparing filter cerebral protection and proximal balloon occlusion. *JACC Cardiovasc Interv* 2014;7:1177–83

12. Sato Y, Ogasawara K, Narumi S, et al. Optimal MR plaque imaging for cervical carotid artery stenosis in predicting the development of microembolic signals during exposure of carotid arteries in endarterectomy: comparison of 4 T1-weighted imaging techniques. *AJNR Am J Neuroradiol* 2016;37:1146–54

13. Yoshida K, Narumi O, Chin M, et al. Characterization of carotid atherosclerosis an ddetection of soft plaque with use of black-blood MR imaging. *AJNR Am J Neuroradiol* 2008;29:868–74

14. Liu XS, Zhao HL, Cao Y, et al.Comparison of carotid atherosclerotic plaque characteristics by high-resolution black-blood MR imaging between patients with first-time and recurrent acute ischemic stroke. *AJNR Am J Neuroradiol* 2012;33:1257–61

15. Yoshimura S, Yamada K, Kawasaki M, et al. High-intensity signal on time-of-flight magnetic resonance angiography indicates carotid plaques at high risk for cerebral embolism during stenting. *Stroke* 2011;42:3132–37

16. Saito A, Sasaki M, Ogasawara K, et al. Carotid plaque signal differ ences amongfourkindsofT1-weightedmagneticresonance imag ing techniques: a histopathological correlation study. *Neuroradiology* 2012;54:1187–94

17. Bradley Jr WG. MR appearance of hemorrhage in the brain. *Radiology* 1993;189:15–26

18. de Rochefort L, Liu T, Kressler B, et al. Quantitative susceptibility map reconstruction from MR phase data using bayesian regularization: validation and application to brain imaging. *Magn Reson Med* 2010;63:194–206

19. Liu T, Surapaneni K, Lou M, et al. Cerebral microbleeds: burden assessment by using quantitative susceptibility mapping. *Radiology* 2012;262:269–68

20. Chang S, Zhang J, Liu T, et al. Quantitative susceptibility mapping of intracerebral hemorrhages at various stages. *J Magn Reson Imaging* 2016;44:420–25

21. Chen W, Zhu W, Kovanlikaya I, et al. Intracranial calcifications and hemorrhages: characterization with quantitative susceptibility mapping. *Radiology* 2014;270:496–505

22. Azuma M, Maekawa K, Yamashita A, et al. Characterization of carotid plaque components by quantitative susceptibility mapping. *AJNR Am J Neuroradiol* 2020; 41:310–17

23. Ikebe Y, IshimaruH, Imai H, et al. Quantitative susceptibility mapping for carotid atherosclerotic plaques: a pilot study. *Magn Reson Med Sci* 2020;19:135–40

24. Wang C, Zhang Y, Du J, et al. Quantitative susceptibility mapping for characterization of intraplaque hemorrhage and calcification in carotid atherosclerotic Disease. *J Magn Reson Imaging* 2020;52:534–41

25. Sun H, Wilman H A. Background field removal using spherical mean value filtering and Tikhonov regularization. *Magn Reson Med* 2014;71:1151–57

26. Shirai T, Sato R, Taniguchi Y, et al. Quantitative susceptibility mapping using adaptive edge-pre-serving filtering. *Proceedings of the 23rd Annual Meeting of ISMRM*, Toronto, 2015; 3319

27. Shirai T, Sato R, Kawata Y, et al. Region expansion of background field removal with local spherical harmonics approximation for whole-brain quantitative susceptibility mapping. *Magn Reson Med Sci* 2023;22:497–514

28. Yamaguchi A, Kudo K, Sato R, et al. Efficacy of quantitative susceptibility mapping with brain surface correction and vein removal for detecting increase magnetic susceptibility in patients with Alzheimer's disease. *Magn Reson Med Sci* 2023;22:87–94

29. Rutgers DR, Blankensteijn JD, van der Grond J. Preoperative MRA flow quantification in CEA patients: flow differences between patients who develop cerebral ischemia and patients who do not develop cerebral ischemia during cross-clamping of the carotid artery. *Stroke* 2000;31:3021–28

Supplemental Materials

On-line MR Plaque Imaging and Data Processing

Eight patients were scanned with the combinations of TEs, numbers of excitationsand acquisition matrix sizes shown below.

Patient	TEs	Number of excitations	Acquisition matrix size
1	3.1/6.1/9.0/12.0/15.0/17.9/20.9/23.8	1	200 × 200
2	3.1/6.1/9.0/12.0/15.0/17.9/20.9/23.8	1	200 × 200
	4.4/ 8.7/13.0/17.3/21.6/ 25.9/30.2/34.5	1	200 × 200
3	3.1/6.1/9.0/12.0/15.0/17.9/20.9/23.8	1	200 × 200
	4.4/ 8.7/13.0/17.3/21.6/ 25.9/30.2/34.5	1	200 × 200
4	3.1/6.1/9.0/12.0/15.0/17.9	1	200 × 200
	3.1/6.1/9.0/12.0/15.0/17.9	2	200 × 200
5	3.1/6.1/9.0/12.0/15.0/17.9	1	200 × 200
	3.1/6.1/9.0/12.0/15.0/17.9	2	200 × 200
6	3.1/6.1/9.0/12.0/15.0/17.9	1	200 × 200
	3.1/6.1/9.0/12.0/15.0/17.9	2	200 × 200
7	3.1/6.1/9.0/12.0/15.0/17.9	1	200 × 200
	3.1/6.1/9.0/12.0/15.0/17.9	1	200 × 200
8	3.1/6.1/9.0/12.0/15.0/17.9	1	200 × 200
	3.1/6.1/9.0/12.0/15.0/17.9	1	200 × 200

Patient 1 was initially scanned using parameters set based on a previous study thatreported QSM for the brain.[1]

Patients 2 and 3 were scanned at two different TEs, and twoinvestigators found that image quality was better in QSM generated using TEs of3.1/6.1/9.0/12.0/15.0/17.9/20.9/23.8 than in that using 4.4/8.7/13.0/17.3/21.6/25.9/30.2/34.5. Further, when QSM images generated using all 8 TEs were compared with those generated using only 6 TEs of 3.1/6.1/9.0/12.0/15.0/17.9, image quality was better in the latter than in the former. Optimal TEs were thus determined to be 3.1/6.1/9.0/12.0/15.0/17.9.

Patients 4, 5 and 6 were scanned at two different numbers of excitations, and two investigators found that utilizing 2 excitations minimally improved image quality on QSM when compared with utilizing 1 excitation. Considering scan time, the optimal number of excitations was determined to be 1.

Patients 7 and 8 were scanned at two different acquisition matrix sizes, and two investigators found that image quality was better in QSM generated using an acquisitionmatrix size of 200 × 200 than in that using 320 × 320. Optimal acquisition matrix size was therefore determined to be 200 × 200.

1. Sato R, Kudo K, Udo N, et al. A diagnostic index based on quantitative susceptibility

mapping and voxel-based morphometry may improve early diagnosis of Alzheimer's disease. *Eur Radiol* 2022;32: 4479–88

On-line Statistical Analysis

Data are expressed as the mean ± standard deviation (SD). Correlations between twovariables were determined using Spearman’s rank correlation coefficient. Differences between two correlation coefficients were compared using the Meng–Rosenthal–Rubin method. Bland–Altman analysis was performed to confirm concordance between RA-histologic IPH and T1WI FSE-RSI or susceptibility. Taking the correlation between different measures in the same patient into account, we evaluated relationships between two variables using generalized linear mixed-effects models with a subject random intercept. These two parameters were assumed to be normal variables with an identity link. Receiver operating characteristic (ROC) curves were used to assess the accuracy ofT1WI FSE-RSI and susceptibility for detecting plaque consisting primarily of IPH. Pair-wise comparisons of areas under the ROC curves for T1WI FSE-RSI and susceptibility were then performed. The exact 95%CIs for sensitivity, specificity, and positive and negative predictive values were computed with binomial distributions. McNemar's chi- squared test with continuity correction was applied to determine whether row and column marginal frequencies were equal (that is, whether "marginal homogeneity" was present) between histologic sections comprising primarily IPH and T1WI FSE-RSI orsusceptibility. For all statistical analyses, significance was set at the level of $P < .05$.

On-line Results

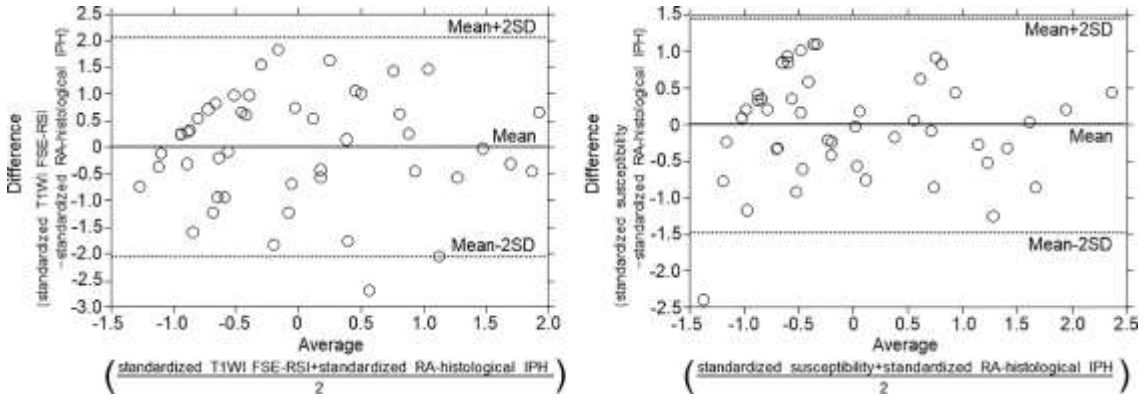

Bland–Altman plots of standardized relative area (RA)-histological intraplaque hemorrhage (IPH) and standardized T1WI FSE-relative signal intensity (RSI) (left graph)or standardized susceptibility value on quantitative susceptibility mapping (right graph) for each histologic section and each MR image. Each value was standardized using the following formula: (a value - mean of referenced group)/SD of referenced group.

On-line Discussion

QSM for carotid plaque has also been used to visualize structures or pathological phenomena other than IPH and calcification. Stone et al. using ex vivo porcine carotid arteries demonstrated that QSM is sensitive to the microstructural composition of arterialvessels, most notably to collagen, suggesting that QSM has potential to provide a sensitiveand specific marker of vessel disease because vessel microstructure becomes increasinglydisrupted during the onset and progression of carotid atherosclerosis.[1] Ruetten et al. obtained QSM before and after administration of ultrasmall superparamagnetic iron oxide nanoparticles, which identify regions of inflammation, for patients with moderate to severe stenosis of the carotid artery and showed that QSM provided positive contrast for plaques demonstrating nanoparticle uptake.[2] This QSM with administration of nanoparticles may allow visualization of the degree of inflammation in carotid plaque.[2]

QSM for carotid plaque has undergone various technical advances. Nguyen et al. developed a nonlinear preconditioned total field-inversion algorithm for robust QSM of carotid plaques and evaluated its performance in comparison with a local field-inversion algorithm previously applied to carotid QSM.[3] As a result, a nonlinear preconditioned total field-inversion algorithm can resolve calcification and IPH in advanced atherosclerotic carotid plaques. Compared with the local field-inversion algorithm, the

nonlinear preconditioned total field-inversion algorithm provided better QSM quality andhas the potential to improve the detection of these plaque components.[3]

1. Stone AJ, Tornifoglio B, Johnston RD, et al. Quantitative susceptibility mapping of carotid arterial tissue ex vivo: Assessing sensitivity to vessel microstructural composition. *Magn Reson Med* 2021;86:2512–27
2. Ruetten PPR, Cluroe AD, Usman A, et al. Simultaneous MRI water-fat separation andquantitative susceptibility mapping of carotid artery plaque pre- and post-ultrasmall superparamagnetic iron oxide-uptake. *Magn Reson Med* 2020;84:686–97
3. Nguyen TD, Wen Y, Du J, et al. Quantitative susceptibility mapping of carotid plaques using nonlinear total field inversion: Initial experience in patients with significant carotid stenosis. *Magn Reson Med* 2020;84:1501–9